Lipogenesis and innate immunity in hepatocellular carcinoma cells reprogrammed by an isoenzyme switch of hexokinases

Laure Perrin-Cocon[1,†], Pierre-Olivier Vidalain[1,†], Clémence Jacquemin[1], Anne Aublin-Gex[1], Keedrian Olmstead[2], Baptiste Panthu[1,3], Gilles J. P. Rautureau[4], Patrice André[1], Piotr Nyczka[5], Marc-Thorsten Hütt[5], Nivea Amoedo[6], Rodrigue Rossignol[6,7], Fabian Volker Filipp[2,8], Vincent Lotteau[1,*‡] Olivier Diaz[1,*‡]

1- CIRI, Centre International de Recherche en Infectiologie, Univ Lyon, Inserm, U1111, Université Claude Bernard Lyon 1, CNRS, UMR5308, ENS de Lyon, 21 Avenue Tony Garnier, F-69007, Lyon, France.
2- Cancer Systems Biology, Institute of Computational Biology, Helmholtz Zentrum München, Ingolstädter Landstraße 1, D-85764, München, Germany.
3- Actual address: Univ Lyon, CarMeN Laboratory, Inserm, INRA, INSA Lyon, Université Claude Bernard Lyon 1, F-69921, Oullins Cedex, France.
4- Université de Lyon, CNRS, Université Claude Bernard Lyon 1, ENS de Lyon, Centre de RMN à Très Hauts Champs (CRMN), FRE 2034, F-69100 Villeurbanne, France.
5- Department of Life Sciences and Chemistry, Jacobs University, Bremen, Germany.
6- CELLOMET, Centre de Génomique Fonctionnelle de Bordeaux, 146 Rue Léo Saignat, F-33000 Bordeaux, France.
7- Univ. Bordeaux, Inserm, MRGM, U1211, F-33076, Bordeaux, France.
8- School of Life Sciences Weihenstephan, Technical University München, Maximus-von-Imhof-Forum 3, D-85354, Freising, Germany.

† These authors contributed equally to this work
‡These authors jointly supervised this work

*** Corresponding authors:**
vincent.lotteau@inserm.fr (ORCID: 0000-0003-0997-3282)
olivier.diaz@inserm.fr (ORCID: 0000-0002-3451-9914)

Keywords
Hepatocellular carcinoma, hexokinase, lipogenesis, innate immunity, lipoproteins.

This PDF file includes:
Main Text
Figures 1 to 7

Abstract

During the cancerous transformation of normal hepatocytes into hepatocellular carcinoma (HCC), the enzyme catalyzing the first rate-limiting step of glycolysis, namely the glucokinase (GCK), is replaced by the higher affinity isoenzyme, hexokinase 2 (HK2). The transcriptomic analysis of HCC tumors shows that highest expression level of *HK2* in tumor lesions is inversely correlated to *GCK* expression, and is associated to poor prognosis for patient survival. To further explore functional consequences of the GCK-to-HK2 isoenzyme switch occurring during carcinogenesis, *HK2* was knocked-out in the HCC cell line Huh7 and replaced by *GCK*, to generate the Huh7-$GCK^{+}/HK2^{-}$ cell line. HK2 knockdown and GCK expression rewired central carbon metabolism, stimulated mitochondrial respiration and restored essential metabolic functions of normal hepatocytes such as lipogenesis, VLDL secretion, glycogen storage. It also reactivated innate immune responses and sensitivity to natural killer cells, showing that consequences of the HK switch extend beyond metabolic reprogramming.

Main Text

Introduction

Hepatocellular carcinoma (HCC) is the most common liver cancer and the fourth leading cause of cancer-related death (1). HCC is closely linked to chronic liver inflammation, chronic viral hepatitis, exposure to toxins, and metabolic dysfunction such as non-alcoholic steatohepatitis (NASH). HCC is of poor prognosis, and treatments are essentially based on surgical resection, liver transplantation or aggressive chemo and/or radiotherapy. In patients with advanced HCC, broad-spectrum kinase inhibitors are approved (2) but with limited benefit (3). Effective personalized therapies are needed but their development is impeded by our poor understanding of molecular mechanisms underlying HCC onset and progression. Efforts to characterize the disease on the

71 basis of etiology and outcomes revealed metabolic deregulation as a hallmark of HCC progression
72 (4). Indeed, metabolic remodeling is critically required for tumor growth, since bioenergetic
73 requirements and anabolic demands drastically increase (5–7). For instance, HCC cells have lost
74 their ability to secrete very low-density lipoproteins (VLDL), a highly specialized function of
75 hepatocyte and can only secrete low-density lipoproteins (LDL)-like lipoproteins, indicating a
76 defective lipogenesis and/or lipoprotein assembly (8).

77 Metabolic reprogramming in cancer cells involves the modulation of several enzymes by
78 oncogenic drivers (6). Targeting these enzymes is now considered as a therapeutic strategy for
79 several types of cancers (6). Among these enzymes, hexokinase 2 (HK2) stands out because of its
80 elevated or induced expression in numerous cancers, including HCC (9). Hexokinases control the
81 first rate-limiting step of glucose catabolism by phosphorylating glucose to glucose-6-phosphate
82 (G6P), fueling glycolysis as well as glycogen, pentose phosphate and triglyceride synthesis. The
83 human genome contains four genes encoding distinct hexokinase isoenzymes, named HK1 to HK4
84 (HK4 is also known as glucokinase or GCK), with distinct enzymatic kinetics and tissue
85 distributions. A fifth putative hexokinase enzyme was recently discovered but has not been fully
86 characterized yet (10). A switch from GCK to HK2 isoenzymes is occurring during the transition
87 from primary to tumor hepatocytes so that HCC cell lines express HK2 but no longer GCK. HK2
88 expression level has been correlated with disease progression and dedifferentiation of HCC cells
89 (11). When HK2 is artificially knocked-down in HCC cell lines, glycolysis is repressed, and
90 tumorigenesis is inhibited while cell death increases (9). In addition, hexokinase function extends
91 beyond metabolism towards autophagy, cell migration, and immunity, suggesting that the GCK-
92 to-HK2 isoenzyme switch has broader consequences than initially suspected (12–15). Here, we
93 analyzed transcriptomic data of HCC biopsies and correlated hexokinase isoenzyme expression

94 level with patient survival. This led us to generate a new human HCC model expressing *GCK*
95 instead of *HK2*. A comparative analysis of *GCK*$^{+}$ *vs* *HK2*$^{+}$ HCC cell lines provided a unique
96 opportunity to look into HK isoenzyme-dependent metabolic features, lipoprotein production and
97 resistance to immune signals of liver cancer cells.

98 ## Results

99 ### Relative expression level of GCK and HK2 in HCC patients

100 Although an isoenzyme switch from GCK to HK2 has been observed during the carcinogenesis
101 process (16), whether hexokinase isoenzymes expression is predictive of patient survival is
102 unclear. We first analyzed the transcriptomes (RNAseq data) of 365 HCC biopsies from The Cancer
103 Genome Atlas (TCGA) database (17, 18)(Supplementary Table 1). For each HK, the individual gene
104 expression level was used to stratify patients into two subgroups according to Uhlen et al. (18)
105 and overall survival in the two subgroups was determined using a Kaplan-Meier's estimator.
106 Although *HK1* or *HK3* expression level were not associated to patient survival rate (Fig. 1a), highest
107 expression levels of *HK2* as previously described (19) and lowest expression levels of *GCK* in the
108 tumors were associated with a lower survival rate. We thus stratified patients based on the
109 GCK/HK2 expression ratio to combine these two markers (Fig. 1b). When patients were stratified
110 on the basis of *HK2* or *GCK* expression levels, the median survival between the corresponding
111 subgroups differed by 33.8 and 36.5 months, respectively (Fig. 1a). This difference reached 42.8
112 months when the stratification of patients was based on the *GCK/HK2* ratio (Fig. 1b). This
113 demonstrated that the *GCK/HK2* ratio outperforms *HK2* or *GCK* expression alone as predictor of
114 patient survival. Finally, correlation coefficients between patient survival in months and *HK2* or
115 *GCK* expression level were determined. For this, we only considered the subset of 130 patients
116 for whom the period between diagnosis and death is precisely known (uncensored data), and

117 performed a Spearman's rank correlation test (Fig. 1c). Patient survival was positively correlated
118 to *GCK* expression but inversely correlated to *HK2* expression in line with the Kaplan-Meier
119 analysis. In addition, *GCK* and *HK2* expression tends to be inversely correlated in tumor samples
120 (Fig. 1c). Therefore, there is a trend for mutual exclusion of *GCK* and *HK2* expression in HCC
121 tumors, and this profile is associated to clinical outcome.

122 **Engineering a cellular model of the hexokinase isoenzyme switch**

123 To decipher functional consequences of GCK or HK2 expression in a HCC model, we restored GCK
124 expression by lentiviral transduction in the reference HCC cell line Huh7, and knocked-out the
125 endogenous *HK2* gene by CRISPR/Cas9. The exclusive expression of HK2 and *GCK* in Huh7 and
126 Huh7-$GCK^+/HK2^-$ cell lines, respectively, was validated, while HK1 and HK3 were not expressed
127 (Fig. 2a). The hexokinase activity in the presence of increasing concentration of glucose was
128 determined in protein lysates from the two respective cell lines. Hexokinase activity in Huh7 lysate
129 reached its maximum at low glucose concentration, presenting a saturation curve according to
130 Michaelis–Menten kinetics (Fig. 2b). In contrast, the hexokinase activity in Huh7-$GCK^+/HK2^-$
131 lysates followed a pseudo-allosteric response to glucose (20, 21). Thus, the expected HK2 and GCK
132 activities were observed in the Huh7 and Huh7-$GCK^+/HK2^-$ cells respectively. The cell proliferation
133 capacity remained identical between the two cell lines (Supplementary Fig. 1). We then compared
134 the genome edited Huh7-$GCK^+/HK2^-$ and the parental Huh7 cell lines (*i.e.* Huh7-$GCK^-/HK2^+$) at a
135 transcriptomic, metabolic and immunological level.

136 **Transcriptomic data revealed extended modifications of metabolic connections in Huh7-**
137 **GCK+/HK2-**

138 Transcriptomic profiles of Huh7 and Huh7-$GCK^+/HK2^-$ cells were determined by next generation
139 sequencing (Supplementary Table 2). Overall, 4.2% of the gene transcripts were reduced and 6.9%

140 were induced in Huh7-*GCK*$^{+}$/*HK2*$^{-}$ compared to Huh7 (Fig. 2c; |fold-change (FC)|>2 and *p*
141 value<0.05). We first determined the metabolic consequences of the HK isoenzyme switch by
142 mapping the differentially expressed genes onto the a well-established bipartite metabolic
143 network Recon2, connecting gene products and metabolites (Supplementary Fig. 2-4) (22, 23).
144 After trimming highest-degree metabolites as currency metabolites, clusters of genes that are
145 both differentially expressed and connected by common metabolites emerged. Interestingly, we
146 found that across a wide range of analysis parameters, including varying rates of currency
147 metabolites and gene expression fold-change, the differentially expressed metabolic genes are
148 substantially better connected than expected by chance (Fig. 2d). This highlights the specificity of
149 the transcriptomic changes with respect to metabolic pathways. The spanned network presented
150 in Figure 2e corresponds to a stringent fold-change threshold for transcriptomic data
151 ($\log_2$(|FC|)>3) while removing 2 percent of highest-degree currency metabolites. This network
152 shows connected components within glycolysis, but also across distant modules including the
153 gamma-aminobutyric acid (GABA) shunt (ALDH5A1), urea cycle (CPS1, OTC), glycogen metabolism
154 (GYS1, GYS2, AGL) and lipid synthesis (GPAM, AGPAT4, DGKG, CDS1, A4GALT) or degradation
155 (ACADL, HSD17B4, AMACR). This analysis highlights the global impact of the HK isoenzyme switch
156 that spreads beyond glycolysis across distant connected metabolic modules.

157 Enrichment of molecular and cellular functions in differentially expressed genes was also analyzed
158 using Ingenuity Pathway Analysis (IPA). This revealed that cellular movement and lipid
159 metabolism were the most affected functions (Fig. 3a and Supplementary Table 3). A closer look
160 at these annotations pointed to differences in the migratory capacities (Fig. 3b) as well as lipid
161 concentration and synthesis (Fig. 3c). The migratory capacities of Huh7 and Huh7-*GCK*$^{+}$/*HK2*$^{-}$ were
162 compared using transwell-migration cell assays (Fig. 3d-e). Results showed a higher migratory

163 capacity of Huh7-*GCK*$^{+}$/*HK2*$^{-}$ cells, in line with Kishore M. et al showing that GCK expression
164 induced by pro-migratory signals controls the trafficking of CD4^{+}/CD25^{+}/FOXP3^{+} regulatory T (T_{reg})
165 cells (15). To validate the differences in lipid metabolism highlighted by the transcriptomic
166 analysis, intracellular content in neutral lipids was first determined with lipophilic dyes. As
167 assessed by Oil-Red-O or BODIPY staining, an accumulation of intracellular neutral lipids was
168 observed in Huh7-*GCK*$^{+}$/*HK2*$^{-}$ in comparison to Huh7 (Fig. 3f and 3g). The accumulation of neutral
169 lipids in Huh7 expressing both *HK2* and *GCK* indicates that the phenotype is driven by *GCK*
170 expression and not by *HK2* knockdown (Supplementary Fig. 5). Lipid accumulation upon GCK
171 expression was also observed in Huh6 hepatoblastoma cells but not in epithelial kidney Vero cells,
172 indicating that this phenomenon occurs in metabolically relevant cells (Supplementary Fig. 5).

173 **Differential lipid metabolism in Huh7 and Huh7-*GCK*$^{+}$/*HK2*$^{-}$**

174 The intracellular lipid content of the two cell lines was further analyzed. In Huh7-*GCK*$^{+}$/*HK2*$^{-}$, an
175 enrichment in phosphatidylcholine, cholesterol, triglycerides (TG) and free fatty acids was
176 observed compared to Huh7 (Fig. 4a). One major function of hepatocytes is to secrete triglyceride-
177 rich VLDL and this function is altered in HCC cells that secrete smaller lipoproteins with the density
178 of LDL (24, 25). The secretion of lipids and lipoproteins by both cell lines was analyzed after a 24h-
179 culture in the absence of FCS to exclude any participation of exogenous lipids in the production
180 of lipoproteins. Huh7-*GCK*$^{+}$/*HK2*$^{-}$ secreted more free fatty acids than Huh7 while secretion of
181 cholesterol and triglycerides (TG) remained unchanged (Fig. 4b). However, under the same
182 conditions, the secretion of apolipoprotein B (ApoB) by Huh7-*GCK*$^{+}$/*HK2*$^{-}$ was reduced compared
183 to Huh7. Since ApoB is a non-exchangeable protein with only one copy in VLDL and LDL particles,
184 an elevated TG/ApoB ratio indicates that ApoB^{+}-lipoproteins secreted by Huh7-*GCK*$^{+}$/*HK2*$^{-}$ cells
185 are enriched in TG compared to those secreted by Huh7 (Fig. 4c). This was confirmed by the ApoB

186 distribution in density gradient fractions. As expected, lipoproteins secreted by Huh7 sediment at
187 the density of LDL, while those secreted by Huh7-*GCK*$^{+}$/*HK2*$^{-}$ (Fig. 4d) match the density of VLDL
188 found in human plasma or secreted by primary human hepatocytes in culture (26, 27). This
189 indicates that GCK expression is essential for the VLDL assembly/secretion pathway and could
190 explain the loss of this crucial metabolic pathway in hepatoma cells expressing HK2 instead of GCK
191 (28).

192 **Differential activity of the tricarboxylic acid cycle (TCA) in Huh7 and Huh7-*GCK*$^{+}$/*HK2*$^{-}$**

193 We observed that GCK expression increased the intracellular content in lipids, resulting in
194 accumulation of lipid droplets and secretion of VLDL. A rewiring of cellular metabolism towards
195 energy storage in Huh7-*GCK*$^{+}$/*HK2*$^{-}$ was thus suspected and confirmed by the accumulation of
196 glycogen, creatinine and creatinine-P (Fig. 5a and b), a feature of functional hepatocytes. To
197 further determine the consequences of replacing HK2 by GCK, we quantified prominent
198 intracellular metabolites via GC-MS. Figure 5c shows relative intracellular quantities of
199 metabolites that are significantly different between Huh7 and Huh7-*GCK*$^{+}$/*HK2*$^{-}$. Among
200 differentially represented metabolites, higher levels of glucose, glycerol-3-phosphate and lactic
201 acid were detected in Huh7-*GCK*$^{+}$/*HK2*$^{-}$ *cells*. Several intermediates of the TCA cycle (succinic acid,
202 fumaric acid, alpha-ketoglutaric acid), and metabolites directly connected to it (GABA, glutamic
203 acid, glutamine, aspartic acid) were also differentially present between the two cell lines. This
204 supports a significant modulation of central carbon metabolism at both the level of glycolysis and
205 TCA cycle. This led to investigate glucose catabolism in further details. Glucose consumption and
206 stable isotope incorporation from [U-^{13}C]-glucose into pyruvate were both increased in Huh7-
207 *GCK*$^{+}$/*HK2*$^{-}$cells compared to Huh7 cells (Fig. 5d and f). This increased glycolytic flux together with
208 a reduced lactate secretion (Fig. 5e) is likely to account for the elevation of lactate levels and

209 suggest that the increased pyruvate production essentially fuels mitochondrial TCA cycle in Huh7-
210 *GCK*$^{+}$*/HK2*$^{-}$cells.

211 Pyruvate entering the mitochondria downstream of glycolysis can be either oxidized by pyruvate
212 dehydrogenase (PDH), producing acetyl-CoA, or converted into oxaloacetate (OAA) by pyruvate
213 carboxylase (PC). Acetyl-CoA and OAA are then combined in the TCA cycle to form citrate. *De novo*
214 lipogenesis requires citrate egress from the TCA cycle to serve as a precursor of cytosolic acetyl-
215 CoA for further synthesis of fatty acids. In Huh7-*GCK*$^{+}$*/HK2*$^{-}$ cells, we observed both an increased
216 activity of PC (Fig. 5g) without changes in protein expression (Fig. 5h) and an increased
217 phosphorylation of pyruvate dehydrogenase (PDH), which is indicative of a reduced activity of this
218 enzyme (Fig. 5i). This is consistent with the increased expression of the PDH kinase PDK2 and the
219 decreased expression of the PDH phosphatase PDP2 in Huh7-*GCK*$^{+}$*/HK2*$^{-}$ cells that regulate the
220 PDH phosphorylation state (Fig. 5j). A rebalanced usage of pyruvate in Huh7-*GCK*$^{+}$*/HK2*$^{-}$ cells
221 maintains a functional TCA cycle and supports lipogenesis. In Huh7-*GCK*$^{+}$*/HK2*$^{-}$ cells, we also
222 observed an increased phosphorylation of ATP citrate lyase (ACLY), the first enzyme of the fatty
223 acid synthesis pathway, indicating an enhanced activity of this enzyme (Fig. 5k). This reaction also
224 regenerates OAA in the cytosolic compartment. Interestingly, transcriptomic data show that PCK1
225 which converts OAA to phosphoenolpyruvate (PEP), is overexpressed in Huh7-*GCK*$^{+}$*/HK2*$^{-}$cells
226 compared to Huh7 (FC > 32).
227 A shift from pyruvate oxidation to carboxylation is observed in cancer cells where succinate
228 dehydrogenase (SDH) is inactivated by mutation and OAA can only be generated through PC
229 activity (29). SDH inhibition leads to succinate accumulation, especially in activated immune cells
230 (30). Interestingly, higher levels of succinate and a reduced activity of SDH were measured in
231 Huh7-*GCK*$^{+}$*/HK2*$^{-}$ cells compared to Huh7 (Fig. 5l and m). Even though SDH is also part of the

232 complex II of the mitochondrial respiratory chain, we observed that the overall oxygen
233 consumption was increased in Huh7-*GCK*$^{+}$/*HK2*$^{-}$ (Fig. 5n) with increased basal and maximal
234 respiration, ATP production and spare respiration capacity (Supplementary Fig. 6). Functional
235 analysis of the respiratory chain showed that oxygen consumption in Huh7 and Huh7-*GCK*$^{+}$/*HK2*$^{-}$
236 cells was mainly dependent on complex I which is fueling complex III (Fig. 5n and o). Thereby, the
237 HK isoenzyme switch rewired the TCA cycle promoting carboxylation of pyruvate into OAA in the
238 presence of a reduced SDH activity and increased respiration through complex I.

239 **Restored innate immune sensitivity in Huh7-*GCK*$^{+}$/*HK2*$^{-}$**

240 Lipid accumulation in hepatocytes is incriminated in hepatic inflammation (31) and TCA cycle
241 rewiring is associated with innate immunity activation (32). These two events were observed
242 when replacing HK2 by GCK in Huh7 cells, questioning the immune status of these cells and their
243 sensitivity to antitumor immunity. The functional analysis of gene ontology (GO) terms associated
244 to differentially expressed transcripts revealed an enrichment in terms related to the regulation
245 of innate immunity. The gene signature associated with type-I interferon (IFN) signaling pathway
246 scored among the top enriched terms of upregulated genes in Huh7-*GCK*$^{+}$/*HK2*$^{-}$ cells
247 (Supplementary Fig. 7). Within the 91 gene members of this GO term, 20 transcripts of Type I-IFN
248 signaling were significantly up-regulated in Huh7-*GCK*$^{+}$/*HK2*$^{-}$ compared to Huh7 (Fig. 6a). This
249 includes interferon regulatory factors (IRF1, IRF7 and IRF9), IFN-stimulated genes (ISGs) such as
250 ISG15, MX1, OAS1, OAS3, RNaseL and signaling intermediates such as IKBKE coding for IKKε (Fig.
251 6b). The chaperon HSP90AB1, which is involved in the phosphorylation and activation of STAT1,
252 was also induced (33). In contrast, two genes were significantly down-regulated in Huh7-
253 *GCK*$^{+}$/*HK2*$^{-}$ compared to Huh7, the RNaseL inhibitor ABCE1, and TRIM6, an E3 ubiquitin-protein
254 ligase regulating IKKε. Among the members of the RIG-I-like receptor (RLR) family involved in

255 immune sensing and antitumor defense (34), the expression of IFIH1 (also known as MDA5) was
256 slightly increased in Huh7-*GCK*$^{+}$/*HK2*$^{-}$, while RIG-I itself remained unchanged. Such identified gene
257 sets suggest that Huh7-*GCK*$^{+}$/*HK2*$^{-}$ cells may be better equipped than Huh7 cells to respond to
258 innate immune signals. Thus, we compared the innate immune response of the two cell lines
259 when stimulated by RIG-I or MDA5 ligands, known to sense different double-stranded RNA
260 (dsRNA) in viral immune recognition. In order to quantify cellular activation by dsRNA, immuno-
261 stimulatory challenge assays were conducted with triphosphate-hairpin RNA (3p-hpRNA) or
262 polyinosinic-polycytidylic acid (poly(I:C)). Interferon-sensitive response element (ISRE)-
263 dependent transcription was efficiently induced by these RLR ligands in Huh7-*GCK*$^{+}$/*HK2*$^{-}$ cells
264 whereas Huh7 response was very limited even at high doses of immuno-stimulatory ligands (Fig.
265 6c).
266 To investigate whether this differential sensitivity to RLR ligands is linked to GCK expression or
267 HK2 knockout, we used Huh7 cells transduced for GCK expression so that they express both HK2
268 and GCK (Huh7-*GCK*$^{+}$/*HK2*$^{+}$). In these cells, the response to RIG-I ligation did not differ from that
269 of Huh7 cells suggesting that GCK expression alone is not sufficient to restore immune sensitivity
270 (Fig. 6d). When HK2 expression was repressed in these cells with a shRNA (Huh7-*GCK*$^{+}$/*HK2*$^{-}$Sh)
271 (see Supplementary Fig. 8 showing 95% extinction of HK2 protein), ISRE response to RIG-I signaling
272 was restored to a level similar to that observed in Huh7-*GCK*$^{+}$/*HK2*$^{-}$ cells (Fig. 6d). This is pointing
273 towards HK2 as a negative regulator of RLR signaling in HCC cells and suggests that the *GCK*-to-
274 *HK2* isoenzyme switch during malignant transformation of hepatocytes is accompanied by a
275 reduced sensitivity to innate immune signals. The higher sensitivity to RLR ligands of Huh7-
276 *GCK*$^{+}$/*HK2*$^{-}$ cells also resulted in increased secretion of inflammatory interleukins (IL-6 and IL-8),
277 antiviral cytokines (IFN-λ_1, IFN-$\lambda_{2/3}$, IFN-β), and IP-10 (Fig. 6e), indicating that both NF-κB- and

278 IRF3-dependent signaling pathways were induced. IL-1β, TNFα, IL-12p70, GM-CSF, IL-10 and IFNγ
279 were not detected in the supernatants of none of the cell lines, whether they were stimulated or
280 not.
281 As natural killer (NK) cell-mediated lysis of tumor cells is crucial for the anti-cancer immune
282 defense, we compared the susceptibility of the two cell lines to NK cells cytotoxicity. Figure 6f
283 shows that Huh7 cells are resistant to NK cell-mediated lysis in contrast to Huh7-*GCK*$^{+}$/*HK2*$^{-}$. Thus,
284 replacing HK2 by GCK restored Huh7 sensitivity to NK cell-mediated lysis. Similar results were
285 obtained when NK cells were pre-activated with IL-2 (Supplementary Fig. 9). Altogether, these
286 results demonstrate that HCC cells expressing HK2 instead of GCK exhibit an impaired response
287 to immune signals and also a strong resistance to NK cells. Significantly, these two observations
288 are in line with clinical data showing that elevated GCK expression is associated with prolonged
289 survival, while elevated HK2 expression coinciding with GCK reduction correlates with shorter
290 overall survival (Fig. 1).

291 **Discussion**

292 Metabolic network rewiring is a hallmark of cancer although for most tumors, mechanisms at the
293 origin of this metabolic reprogramming have not been elucidated. While GCK, but not HK2, is
294 expressed in normal hepatocytes, the expression of HK2 occurs during cirrhosis and increases as
295 the disease progresses to carcinoma. Several signaling pathways such as hypoxia inducible factors
296 (HIF), peroxisome proliferator-activated receptors (PPAR) and phosphatidylinositol-4,5-
297 bisphosphate 3-kinase (PI3K) might contribute to HK2 induction in fatty liver disease and its
298 evolution towards cirrhosis and carcinogenesis (35–37). Consequently HK2 induction has been
299 proposed as a risk marker of HCC development (16). Analyzing TCGA data from human HCC
300 tumors, we observed that not only high levels of *HK2* but also low levels of *GCK* are of poor

301 prognosis. In contrast, neither *HK1* nor *HK3* expression levels were correlated with survival of HCC
302 patients. *GCK* expression is very low or not detected in biopsies from a majority of patients (65.8%
303 of patients show RSEM values <10), whereas *HK2* is widely expressed (16) (only 5.8% of patients
304 show RSEM values <10). This probably explains that HK2 expression is a better prognostic marker
305 than GCK for HCC. However, when GCK and HK2 expression were combined into a single ratio,
306 this prognostic marker outperformed HK2 or GCK expression alone. This suggests that both HK2
307 induction and GCK loss play a role in HCC progression. As HK2 and GCK expression tend to be
308 mutually exclusive, both HK2 induction and GCK downregulation might have consequences on the
309 metabolic reprogramming during malignant transformation of hepatocytes. To compare the
310 functional consequences of the HK isoenzyme switch in HCC, we therefore expressed GCK in the
311 reference HCC cell line Huh7 and knocked-down HK2 expression. Our comparative transcriptomic,
312 metabolic and functional studies demonstrate that the replacement of HK2 by GCK not only
313 restored some essential metabolic functions of normal hepatocytes such as lipogenesis, VLDL
314 secretion and glycogen storage but also reactivated innate immune responses and sensitivity to
315 NK-mediated cell lysis.
316 HCC cell lines predominantly secrete LDL-like particles, unlike normal hepatocytes, which secrete
317 VLDL. Lipid loading of Huh7 cells with oleic acid can boost the secretion of $ApoB^+$ particles but
318 does not induce a shift from LDL to VLDL density, indicating that intracellular fatty acid
319 accumulation of exogenous origin cannot rescue VLDL production (28). Here we show that
320 replacing HK2 by GCK in Huh7 cells restored *de novo* fatty acid synthesis, allowing VLDL
321 assembly/secretion in the absence of exogenous lipids. To our knowledge Huh7-$GCK^+/HK2^-$ is the
322 first human cell model with a functional VLDL secretion pathway. Such a tool will strongly benefit
323 the field of cardiovascular diseases and hepatic steatosis.

324 *De novo* fatty acid synthesis from carbohydrates requires an adequate supply in metabolic
325 substrates, especially citrate that is produced by the TCA cycle from incoming pyruvate. The
326 glycolytic entry point into the TCA cycle is controlled by PDH and PC that convert pyruvate into
327 acetyl-CoA or OAA, respectively. Our data revealed that in addition to the increased production
328 of pyruvate from glucose, PC activity is increased whereas PDH is inhibited. This suggests that
329 pyruvate metabolism is rebalanced in favor of OAA in Huh7-*GCK*$^{+}$/*HK2*$^{-}$ cells, as described in
330 healthy liver. Such a mechanism of anaplerosis is known to replenish TCA cycle intermediates and
331 compensate citrate export out of the mitochondria for lipogenesis fueling. Increased PC activity
332 is observed in both normal and pathological situations, mainly as a result of an increased
333 transcription of the PC gene. In our model, mRNA and protein levels were not affected, indicating
334 that PC activity can be regulated by alternative mechanisms depending on HK isoenzyme
335 expression. This may relate to lower levels of oxalate, a known inhibitor of PC activity, in Huh7-
336 *GCK*$^{+}$/*HK2*$^{-}$ cells (Fig. 5c and Fig. 7 discussed below).
337 A rebalanced pyruvate usage in favor of OAA is also described for instance in SDH-deficient
338 neuroendocrine tumor cells, where succinate accumulates and PC activity is increased to maintain
339 OAA production, replenish the oxidative TCA cycle and support aspartate synthesis (29).
340 Interestingly, in comparison to Huh7 cells, succinate and aspartate levels are elevated in Huh7-
341 *GCK*$^{+}$/*HK2*$^{-}$ where SDH activity is reduced, suggesting a direct link between PC and SDH activity in
342 hepatocytes. Several mechanisms inhibiting SDH have been described (38). Modification of the
343 expression of SDH subunits is unlikely as no variation was observed at the transcriptomic level.
344 Itaconate is a weak inhibitor of SDH produced by IRG1 from aconitate but this metabolite was not
345 detected and IRG1 mRNA was absent from the transcriptome of both cell lines. Whether fumarate
346 or other metabolites are responsible for the reduced SDH activity in GCK-expressing cells remains

347 to be investigated. Finally, SDH-deficient cells and LPS-stimulated macrophages have been shown
348 to elicit a hypoxic-like phenotype through accumulation of large amounts of succinate and
349 stabilization of HIF-1α (39, 40). Despite an elevated succinate steady-state level in Huh7-
350 *GCK*$^{+}$*/HK2*$^{-}$ compared to Huh7 cells, we observed no difference in HIF-1α stabilization neither at
351 basal level nor upon induction (Supplementary Fig. 10). This suggested that the reduction of SDH
352 activity in Huh7-*GCK*$^{+}$*/HK2*$^{-}$ cells was not strong enough to induce such a pseudo-hypoxic
353 phenotype.
354 Our gene-centric metabolic analysis of transcriptomic data revealed a wide spreading of
355 metabolic modifications resulting from HK isoenzyme switch. Illustrating these modifications,
356 Figure 7 is an attempt to integrate the observed changes in central carbon metabolism and closely
357 connected metabolic pathways. In particular, decreased level of alanine and increased aspartate
358 concentration in Huh7-*GCK*$^{+}$*/HK2*$^{-}$ cells could be an indirect effect of PC activation that uses
359 pyruvate for the synthesis of OAA. As a consequence, hepatic transaminases may balance
360 intracellular pools of OAA, aspartate, alanine and pyruvate. Glutamate and GABA levels were also
361 modified, thus supporting anaplerosis of the TCA cycle through glutamine consumption and the
362 GABA shunt pathway, respectively. We also observed lower levels of oxalate, an end-product of
363 glyoxylate degradation. In Huh7-*GCK*$^{+}$*/HK2*$^{-}$ *cells,* increased levels of the enzyme alanine-
364 glyoxylate and serine-pyruvate aminotransferase (AGXT) could account for this phenotype as it
365 converts alanine and glyoxylate into pyruvate and glycine, which is also increased. Interestingly,
366 high level of AGXT is a good prognostic marker for HCC (41). Consistently, it was found that oxalate
367 inhibits liver PC, resulting in reduced gluconeogenesis and lipogenesis (42, 43). Thus, a higher PC
368 activity could be explained by lower levels of oxalate in Huh7-*GCK*$^{+}$*/HK2*$^{-}$ cells. We also observed
369 that isoleucine and valine levels increased while BCAT1 (branched chain amino acid transaminase

370 1) predominant transcripts decreased. This suggests a reduced catabolism of branched chain
371 amino acids in Huh7-*GCK*$^{+}$/*HK2*$^{-}$ cells. Again, low levels of BCAT1 is a good prognostic marker for
372 HCC and oral supplementation with branched chain amino acids has been shown to reduce the
373 risk of liver cancer in cirrhotic patients (44, 45). If some metabolic modifications seem to advocate
374 for the restoration of a normal hepatocyte phenotype following the replacement of HK2 by GCK,
375 it cannot be a general statement. Indeed, the urea cycle was also impacted in Huh7-*GCK*$^{+}$/*HK2*$^{-}$
376 cells with lower levels of CPS1 and OTC, which are also observed in aggressive HCC tumors (46).
377 Altogether, our results demonstrate the broad impact of replacing HK2 by GCK in HCC cells, and
378 the key role played by the HK isoenzyme switch in HCC tumor metabolism.
379 We discovered that HK isoenzyme expression not only controls hepatic metabolic functions but
380 also interferes with intrinsic innate immunity of hepatocytes and antitumor immune surveillance.
381 Several reports have recently established functional links between glucose metabolism and
382 signaling pathways downstream of innate immunity sensors of the RLR family, RIG-I and MDA5
383 (47–49), which are usually associated with antiviral responses. However, RIG-I expression is
384 downregulated in hepatic cancer tissues and low RIG-I expression is correlated with poor survival
385 of patients, whereas RIG-I expression in HCC cell lines enhanced IFN response and cancer cell
386 apoptosis (34). This suggests an unexpected role of this receptor family in the antitumor response.
387 Here we show that Huh7 cells expressing GCK instead of HK2 exhibit a higher sensitivity to RIG-I
388 and MDA5 ligands, and produce higher levels of type I/III IFNs and inflammatory cytokines. This
389 immune phenotype occurs in a context of reduced SDH activity and increased intracellular content
390 in succinate (Fig. 5l-m). A pro-inflammatory function of immune cells such as macrophages was
391 previously linked to TCA rewiring, with reduced SDH activity resulting in succinate accumulation
392 (39, 50, 51). Succinate can also be secreted from LPS-activated macrophages and activate its

393 cognate receptor, succinate receptor 1 (SUCNR1, previously known as GPR91) in an autocrine and
394 paracrine manner to further enhance production of IL-1β (52). Interestingly, glucose metabolism
395 promotes RIG-I and MDA5 signaling through the O-GlcNAcylation of the mitochondrial adaptor
396 MAVS (47). Thus, an intriguing hypothesis is that GCK expression could facilitate MAVS signaling
397 by increasing UDP-GlcNAc through upregulation of the hexosamine biosynthetic pathway. HK2
398 binding at the surface of mitochondria may also compete with pyruvate carboxylase, metabolites
399 or mitochondria factors known to control MAVS signaling (47–49). Here we show that HK2
400 knockdown promotes RIG-I-induced ISRE-dependent transcription (Fig. 6d). This is consistent with
401 the results obtained by Zhang W. et al. (48), indicating that HK2 interaction with MAVS restrains
402 RIG-I-induced IFN-β secretion. Further investigations are now required to decipher the molecular
403 links between metabolism and immune responses.
404 Beyond the inhibition of RLR signaling, other mechanisms might contribute to tumor escape from
405 immune surveillance in HCC patients. In advanced-stage HCC patients, NK cells often exhibit
406 reduced infiltration and impaired functional activities (53). We thus compared the sensitivity of
407 Huh7-*GCK*$^{+}$/*HK2*$^{-}$ cells to Huh7, and found that sensitivity to NK cell lysis is restored when HK2 is
408 replaced by GCK. When analyzing cell surface expression of the NK cells inhibitors, HLA class I and
409 MICA/B, no significant changes were observed between cell lines (Supplementary Fig. 9). In
410 contrast, an increased transcription and surface expression of ICAM1 (FC=2.6; Supplementary Fig.
411 9) was observed in Huh7-*GCK*$^{+}$/*HK2*$^{-}$. Since ICAM-1 binding to active LFA-1 at the surface of NK
412 cells is essential for granule polarization and efficient killing of the target cells (54), its enhanced
413 exposition at the surface of Huh7-*GCK*$^{+}$/*HK2*$^{-}$ may contribute to their higher sensitivity to NK cell-
414 mediated killing. These results suggest that HK2 expression at the expense of GCK in HCC tumors

415 decreases immune responsiveness and sensitivity to NK cytotoxicity, thus favoring immune
416 escape.

417 Taken together, our data demonstrate that beyond glycolysis, the hexokinase isoenzyme switch
418 in an HCC model rewires central carbon metabolism, promotes lipogenesis, enhances innate
419 immune functions, and restores sensitivity to natural killer cells.

420

421 **Materials and Methods**
422
423 **Materials.** Unless otherwise specified, chemicals were from Merck Sigma-Aldrich. The RIG-I
424 specific ligand 3p-hpRNA and the MDA5/TLR3 ligand poly(I:C) HMW (High Molecular Weight) were
425 from Invivogen.
426 **Cell cultures.** Huh7 cells and derivatives were grown as previously described (55) in DMEM, 10%
427 fetal calf serum (FCS), penicillin/streptomycin, 1 mM pyruvate, 2 mM L-glutamine. Culture
428 medium and additives were from Gibco except FCS (Dominique Dutcher).
429 **Cell lines**. $15x10^4$ Huh7 cells were transduced for GCK expression at different multiplicities of
430 infection (lentiviral transduction using the pLEX-GCK construct). The Huh7-$GCK^+/HK2^+$ cells were
431 then cultured for 7 days with puromycin (1 µg/mL) before amplification. HK2 knock-out was
432 achieved using the CRISPR/Cas9 system as previously described (56) to obtain Huh7-$GCK^+/HK2^-$
433 cells. A single guide RNA (sgRNA) pair was designed for double nicking using the CRISPR Design
434 Tool (http://tools.genome-engineering.org). The guide sequence oligos ($sgRNA_1$(*HK2*): 5'-
435 CACCGTGACCACATTGCCGAATGCC-3' and $sgRNA_2$(*HK2*): 5'-CACCGTTACCTCGTCTAGTTTAGTC-3')
436 were cloned into a plasmid containing sequences for Cas9 expression and the sgRNA scaffold
437 (pSpCas9(BB)-2A-GFP, Addgene plasmid #48138). 48 h post-transfection, cells were sorted by

438 FACS based on the transient expression of GFP and cloned by limiting dilution. Effective deletion
439 of HK2 was assessed by qPCR.
440 For *HK2* knock-down, Huh7-*GCK*$^{+}$/*HK2*$^{+}$ cells were transduced with lentiviral vectors expressing
441 HK2-targeting shRNAs, and antibiotic selection was applied (hygromycin; 100 µg/ml). The *HK2*-
442 targeting sequence 5'-
443 CCGGCCAGAAGACATTAGAGCATCTCTCGAGAGATGCTCTAATGTCTTCTGGTTTTTT-3' was cloned in
444 the pLKO.1 hygro vector (a gift from Bob Weinberg; Addgene plasmid #24150). HK2 expression in
445 Huh7-*GCK*$^{+}$/*HK2*$^{+}$ and Huh7-*GCK*$^{+}$/*HK2*$^{-}$*Sh* was analyzed on cell lysates by western blotting
446 (Supplementary Fig. 8).
447 **Enzymatic activity assays.** Cells were trypsinized, washed twice, and cell pellets were stored at -
448 80°C. Protein extractions and assays were performed as previously described for hexokinase (57–
449 59) and pyruvate carboxylase (60). Specific enzymatic assays are described in Supplementary
450 Methods.
451 **Metabolomics profiling.** Cells were seeded at $13x10^5$ cells in $75cm^2$ dishes. After 24 h, culture
452 medium was replaced and cells were further incubated during 24 h. Culture supernatants were
453 collected and stored at -80°C. Cells were harvested, washed twice with ice-cold PBS, and cell
454 pellets were stored at -80°C. To analyze catabolic glucose flux, cells were incubated with [U-^{13}C]-
455 glucose (Sigma-Aldrich; 389374-2G) at 12.5 mM and unlabeled glucose at 12.5 mM for 24h.
456 Extraction, separation and analysis of the metabolites by GC-MS are described in Supplementary
457 Methods.
458 **Transcriptome profiling of Huh7 and Huh7-*GCK*$^{+}$/*HK2*$^{-}$ cell lines.** Transcriptome profiling was
459 performed by next generation sequencing (Profilexpert, Lyon). To identify differentially expressed
460 genes, raw data were processed using the DESeq2 analysis pipeline (61). See Supporting

461 Information and Gene Expression Omnibus database with the accession number GSE144214 for
462 entire raw data.

463 **Pathway analysis.** The list of transcripts differentially expressed in Huh7 and Huh7-*GCK*$^{+}$/*HK2*$^{-}$ cell
464 lines was analyzed by gene set enrichment analysis (IPA, Build version: 486617M, Qiagen)
465 weighted by their corresponding fold-change and *p* value. The fold-change cut-off of mean
466 expression for each transcript was set at 2 with an adjusted *p* value<0.05. The list of genes
467 associated with "Type I-IFN signaling pathway" was defined in the AmiGO 2 database. Expression
468 data of these genes were retrieved from the transcriptomes of Huh7-*GCK*$^{+}$/*HK2*$^{-}$ and Huh7, and
469 correspond for each gene to the most differentially expressed transcript.

470 **Cell migration assay.** $2x10^4$ cells were plated in the upper chamber of transwells (Sarstedt, PET
471 8.0-µm, TL - 833932800) with DMEM without FCS to allow migration for 24 h at 37°C. DMEM with
472 10% FCS was distributed in each well, below the chamber. Chambers were gently picked up before
473 a brief PBS rinse and 0.05% crystal violet coloration. The migrated cells were analyzed a Leica M50
474 microscope using a magnification factor of 20x. The number of cells that have migrated through
475 the membrane and attached on the underside of the membrane were counted using the software
476 Image J.

477 **Respiration Assay.** Respiration was measured using an Extracellular Flux Analyzer (Seahorse
478 Bioscience). The assay was performed according to the Agilent Seahorse XF Cell Mito Stress Test
479 as detailed in Supplementary Methods. The number of cells was determined at the end of the run
480 using the SRB assay as previously described (62) or in plate cell counting by Cytation 1 imaging
481 reader (Biotek).

482 **Intracellular lipid staining.** For microscopic observations, cells were fixed 48 h post-seeding, and
483 intracellular lipids stained with Oil-Red-O as described in Supplementary Methods. For the

484 quantification of intracellular lipid droplets by FACS, cells were stained with the 4,4-difluoro-
485 1,3,5,7,8-Pentamethy-4-Bora-3a,4a-Diaza-s-indacene (BODIPY) 493/503 dye (Tocris Bio-Techne).
486 **Protein, ApoB, and Lipid Quantification**. Protein concentration was determined using the DC
487 Protein Assay (Bio-Rad). ApoB concentration in medium and gradients fractions was determined
488 by ELISA as previously described (63). Total concentrations of cholesterol, phospholipids, and
489 triglycerides (TG) were determined using specific assays from Millipore Sigma-Aldrich (ref.
490 MAK043, MAK122 and MAK266 respectively). Free Fatty Acids were quantified using a specific
491 assay kit from Abcam (ref. ab65341).
492 **Iodixanol density gradients.** Iodixanol gradients were prepared as previously described (64). One
493 ml of culture supernatant was applied to the top of 6 to 56% iodixanol gradients and centrifuged
494 for 10h at 41,000rpm and 4°C in a SW41 rotor. The gradient was harvested by tube puncture from
495 the bottom and collected into 22 fractions (0.5 ml each). The density of each fraction was
496 determined by weighing.
497 **Metabolic network coherence computational analysis.** In order to measure the consistency of
498 differentially expressed genes with a metabolic network, we employed the metabolic network
499 coherence measure introduced by Sonnenschein *et al.* (65) (see Supplementary Methods for
500 details). This approach was previously applied to various disease-related transcriptome profiles
501 (66, 67) and for extracting information on the genetic control of metabolic organization (68).
502 Recently, detailed theoretical analysis of the extended version of the method has been performed
503 by Nyczka and Hütt (69)
504 **Western-Blot Analysis.** Protein expression was determined by standard western-blot analysis
505 (See Supplementary Methods for details).
506 **RLR stimulation**

507 Cells were seeded in 96-well or 24-well plates. After 24 h, cells were co-transfected with indicated
508 doses of the RIG-I ligand 3p-hpRNA or the MDA5/TLR3 ligand poly(I:C) HMW together with the
509 pISRE-luc (1.25 µg/ml) and pRL-SV40 (0.125 µg/ml) reporter plasmids using the JetPEI-Hepatocyte
510 reagent (Polyplus Transfection). Manufacturer's instructions were followed. After 48 h,
511 supernatants were collected for cytokine quantification. Firefly and Renilla luciferase expressions
512 within cells were determined using the Dual-Glo luciferase Assay system (Promega) and an Infinite
513 M200 microplate reader (TECAN).

514 **Cytokine assays**

515 Clarified culture supernatants were collected and stored at -20°C. IL-8 was quantified using the
516 Cytometric Bead Array for human IL-8 (BD Biosciences). Other cytokines were assayed using the
517 LEGENDPlex multiplex assay (Human Anti-Virus Response Panel, BioLegend). Fluorescence was
518 analyzed using a FACS Canto II (BD Biosciences).

519 **NK cell cytotoxicity test**

520 NK cells were isolated as described in Supplementary Methods from human buffy coats of healthy
521 donors obtained from the Etablissement Français du Sang. Informed consent was obtained from
522 donors and experimental procedures were approved by the local institutional review committee.
523 Huh7 or Huh7-*GCK*$^{+}$/*HK2*$^{-}$ were seeded at $1x10^5$ cells per well in a 24-well plate in RPMI-1640
524 (Gibco) with 10% FCS and 40 µg/ml gentamycin. After 24 h, $3x10^5$ or $3x10^6$ NK cells were added
525 to the culture wells. The cytotoxicity assay was performed for 4 h at 37°C, under 5% CO_2. Target
526 hepatoma cells were harvested after trypsination, labelled with propidium iodide (PI) and
527 analyzed by FACS. Cell death was monitored after morphological gating on hepatocytes.

528 **Statistics and reproducibility**

529 All the statistical analyses were performed with GraphPad Prism or Analyse-it softwares. Details
530 of statistical analyses can be found in figure legends.

531 Acknowledgments

532

533 We acknowledge the contribution of the Genomics and Microgenomics platform ProfileXpert
534 (University Lyon 1, SFR santé LYON-EST, UCBL-Inserm US 7-CNRS UMS3453) and SFR Biosciences
535 (UMS3444/CNRS, US8/Inserm, ENS de Lyon, UCBL) facilities: AniRA-Cytometry, AniRA-ImmOs
536 metabolic phenotyping and LYMIC-PLATIM microscopy. We gratefully thank Laurence Canaple for
537 technical assistance. This work was supported by the Fondation pour la Recherche Médicale
538 (FRM), grant number DEQ20160334893 to VL. F.V.F. is grateful for the support by grants
539 CA154887, GM115293, CRN-17-427258, NSF GRFP, and the Science Alliance on Precision
540 Medicine and Cancer Prevention by the German Federal Foreign Office, implemented by the
541 Goethe-Institute, Washington, DC, USA, and supported by the Federation of German Industries
542 (BDI), Berlin, Germany.

543 Author Contributions

544 L.P-C., P-O.V., O.D., V.L. designed the experiments with critical advices from G.J.P.R., P.A., R.R. and
545 F.V.F.; C.J., A.A-G., K.O., B.P., G.J.P.R., N.A, R.R. and F.V.F. performed experiments and analyzed
546 the data; P.N. and M-T.H. performed metabolic network computational analysis; L.P-C., P-O.V.,
547 P.A., F.V.F, V.L. and O.D. analyzed the data, prepared figures and wrote the manuscript.
548

549 References

550

551 1. A. Villanueva, Hepatocellular Carcinoma. *N. Engl. J. Med.* **380**, 1450–1462 (2019).

552 2. M. Kudo, *et al.*, Lenvatinib versus sorafenib in first-line treatment of patients with
553 unresectable hepatocellular carcinoma: a randomised phase 3 non-inferiority trial. *The*
554 *Lancet* **391**, 1163–1173 (2018).

555 3. J. M. Llovet, R. Montal, D. Sia, R. S. Finn, Molecular therapies and precision medicine for
556 hepatocellular carcinoma. *Nat Rev Clin Oncol* **15**, 599–616 (2018).

557 4. S. De Matteis, *et al.*, Aberrant Metabolism in Hepatocellular Carcinoma Provides
558 Diagnostic and Therapeutic Opportunities. *Oxidative Medicine and Cellular Longevity* **2018**,
559 1–13 (2018).

560 5. F. V. Filipp, *et al.*, Glutamine-fueled mitochondrial metabolism is decoupled from glycolysis
561 in melanoma. *Pigment Cell & Melanoma Research* **25**, 732–739 (2012).

562 6. N. Hay, Reprogramming glucose metabolism in cancer: can it be exploited for cancer
563 therapy? *Nat Rev Cancer* **16**, 635–649 (2016).

564 7. M. G. Vander Heiden, L. C. Cantley, C. B. Thompson, Understanding the Warburg effect:
565 the metabolic requirements of cell proliferation. *Science* **324**, 1029–1033 (2009).

566 8. J. Jiang, P. Nilsson-Ehle, N. Xu, Influence of liver cancer on lipid and lipoprotein
567 metabolism. *Lipids Health Dis* **5**, 4 (2006).

568 9. D. DeWaal, *et al.*, Hexokinase-2 depletion inhibits glycolysis and induces oxidative
569 phosphorylation in hepatocellular carcinoma and sensitizes to metformin. *Nature*
570 *Communications* **9**, 446 (2018).

571 10. C. Guo, *et al.*, Coordinated regulatory variation associated with gestational hyperglycaemia
572 regulates expression of the novel hexokinase HKDC1. *Nat Commun* **6**, 6069 (2015).

573 11. G. Guzman, *et al.*, Evidence for Heightened Hexokinase II Immunoexpression in
574 Hepatocyte Dysplasia and Hepatocellular Carcinoma. *Dig Dis Sci* **60**, 420–426 (2015).

575 12. A. J. Wolf, *et al.*, Hexokinase Is an Innate Immune Receptor for the Detection of Bacterial
576 Peptidoglycan. *Cell* **166**, 624–636 (2016).

577 13. V. P. Tan, S. Miyamoto, HK2/hexokinase-II integrates glycolysis and autophagy to confer
578 cellular protection. *Autophagy* **11**, 963–964 (2015).

579 14. D. J. Roberts, V. P. Tan-Sah, E. Y. Ding, J. M. Smith, S. Miyamoto, Hexokinase-II Positively
580 Regulates Glucose Starvation-Induced Autophagy through TORC1 Inhibition. *Mol. Cell* **53**,
581 521–533 (2014).

582 15. M. Kishore, *et al.*, Regulatory T Cell Migration Is Dependent on Glucokinase-Mediated
583 Glycolysis. *Immunity* **47**, 875-889.e10 (2017).

584 16. N. C. W. Lee, M. A. Carella, S. Papa, C. Bubici, High Expression of Glycolytic Genes in
585 Cirrhosis Correlates With the Risk of Developing Liver Cancer. *Front Cell Dev Biol* **6**, 138
586 (2018).

587 17. M. Uhlén, *et al.*, Tissue-based map of the human proteome. *Science* **347** (2015).

588 18. M. Uhlen, *et al.*, A pathology atlas of the human cancer transcriptome. *Science* **357** (2017).

589 19. J.-J. Yoo, *et al.*, Hexokinase-II Inhibition Synergistically Augments the Anti-tumor Efficacy of
590 Sorafenib in Hepatocellular Carcinoma. *Int J Mol Sci* **20** (2019).

591 20. C. M. Porter, B. G. Miller, Cooperativity in monomeric enzymes with single ligand-binding
592 sites. *Bioorganic Chemistry* **43**, 44–50 (2012).

593 21. M. Larion, R. K. Salinas, L. Bruschweiler-Li, B. G. Miller, R. Brüschweiler, Order–Disorder
594 Transitions Govern Kinetic Cooperativity and Allostery of Monomeric Human Glucokinase.
595 *PLoS Biology* **10**, e1001452 (2012).

596 22. I. Thiele, *et al.*, A community-driven global reconstruction of human metabolism. *Nat.*
597 *Biotechnol.* **31**, 419–425 (2013).

598 23. D. C. Zielinski, *et al.*, Pharmacogenomic and clinical data link non-pharmacokinetic
599 metabolic dysregulation to drug side effect pathogenesis. *Nature Communications* **6**, 7101
600 (2015).

601 24. G. van den Berghe, The role of the liver in metabolic homeostasis: Implications for inborn
602 errors of metabolism. *Journal of Inherited Metabolic Disease* **14**, 407–420 (1991).

603 25. J. M. Berg, J. L. Tymoczko, L. Stryer, Each Organ Has a Unique Metabolic Profile.
604 *Biochemistry. 5th edition* (2002) (January 13, 2020).

605 26. F. Beilstein, *et al.*, Lysophosphatidylcholine acyltransferase 1 is downregulated by hepatitis
606 C virus: impact on production of lipo-viro-particles. *Gut* **66**, 2160–2169 (2017).

607 27. H. N. Ginsberg, LIPOPROTEIN PHYSIOLOGY. *Endocrinology and Metabolism Clinics of North*
608 *America* **27**, 503–519 (1998).

609 28. S. J. R. Meex, U. Andreo, J. D. Sparks, E. A. Fisher, Huh-7 or HepG2 cells: which is the better
610 model for studying human apolipoprotein-B100 assembly and secretion? *J. Lipid Res.* **52**,
611 152–158 (2011).

612 29. C. Lussey-Lepoutre, *et al.*, Loss of succinate dehydrogenase activity results in dependency
613 on pyruvate carboxylation for cellular anabolism. *Nat Commun* **6**, 8784 (2015).

614 30. V. Lampropoulou, *et al.*, Itaconate Links Inhibition of Succinate Dehydrogenase with
615 Macrophage Metabolic Remodeling and Regulation of Inflammation. *Cell Metab.* **24**, 158–
616 166 (2016).

617 31. A. Mansouri, C.-H. Gattolliat, T. Asselah, Mitochondrial Dysfunction and Signaling in
618 Chronic Liver Diseases. *Gastroenterology* **155**, 629–647 (2018).

619 32. E. L. Mills, B. Kelly, L. A. J. O'Neill, Mitochondria are the powerhouses of immunity. *Nature*
620 *Immunology* **18**, 488 (2017).

621 33. M. Cheng, *et al.*, Stat1 mediates an auto-regulation of hsp90β gene in heat shock
622 response. *Cellular Signalling* **22**, 1206–1213 (2010).

623 34. J. Hou, *et al.*, Hepatic RIG-I predicts survival and interferon-α therapeutic response in
624 hepatocellular carcinoma. *Cancer Cell* **25**, 49–63 (2014).

625 35. G. Panasyuk, *et al.*, PPARγ contributes to PKM2 and HK2 expression in fatty liver. *Nat*
626 *Commun* **3**, 672 (2012).

627 36. O. A. Mesarwi, *et al.*, Hepatocyte Hypoxia Inducible Factor-1 Mediates the Development of
628 Liver Fibrosis in a Mouse Model of Nonalcoholic Fatty Liver Disease. *PLoS One* **11** (2016).

629 37. D. J. Roberts, S. Miyamoto, Hexokinase II integrates energy metabolism and cellular
630 protection: Akting on mitochondria and TORCing to autophagy. *Cell Death and*
631 *Differentiation* **22**, 248–257 (2015).

632 38. J. Van den Bossche, L. A. O'Neill, D. Menon, Macrophage Immunometabolism: Where Are
633 We (Going)? *Trends in Immunology* **38**, 395–406 (2017).

634 39. G. M. Tannahill, *et al.*, Succinate is an inflammatory signal that induces IL-1β through HIF-
635 1α. *Nature* **496**, 238–242 (2013).

636 40. K. Kluckova, D. A. Tennant, Metabolic implications of hypoxia and pseudohypoxia in
637 pheochromocytoma and paraganglioma. *Cell Tissue Res.* **372**, 367–378 (2018).

638 41. Y. Sun, *et al.*, Loss of alanine-glyoxylate and serine-pyruvate aminotransferase expression
639 accelerated the progression of hepatocellular carcinoma and predicted poor prognosis. *J*
640 *Transl Med* **17**, 390 (2019).

641 42. E. A. Yount, R. A. Harris, Studies on the inhibition of gluconeogenesis by oxalate. *Biochim.*
642 *Biophys. Acta* **633**, 122–133 (1980).

643 43. I. E. O'Neill, D. W. Bannister, The effects of oxalate and glucose on lipogenesis by isolated
644 hepatocytes from normal and biotin-deficient chicks (Gallus domesticus). *Int. J. Biochem.*
645 **16**, 517–521 (1984).

646 44. Y. Muto, *et al.*, Overweight and obesity increase the risk for liver cancer in patients with
647 liver cirrhosis and long-term oral supplementation with branched-chain amino acid
648 granules inhibits liver carcinogenesis in heavier patients with liver cirrhosis. *Hepatol. Res.*
649 **35**, 204–214 (2006).

650 45. T. Kawaguchi, *et al.*, Branched-chain amino acids prevent hepatocarcinogenesis and
651 prolong survival of patients with cirrhosis. *Clin. Gastroenterol. Hepatol.* **12**, 1012-1018.e1
652 (2014).

653 46. A. Ally, *et al.*, Comprehensive and Integrative Genomic Characterization of Hepatocellular
654 Carcinoma. *Cell* **169**, 1327-1341.e23 (2017).

655 47. T. Li, *et al.*, O-GlcNAc Transferase Links Glucose Metabolism to MAVS-Mediated Antiviral
656 Innate Immunity. *Cell Host Microbe* **24**, 791-803.e6 (2018).

657 48. W. Zhang, *et al.*, Lactate Is a Natural Suppressor of RLR Signaling by Targeting MAVS. *Cell*
658 **178**, 176-189.e15 (2019).

659 49. Z. Cao, *et al.*, Pyruvate Carboxylase Activates the RIG-I-like Receptor-Mediated Antiviral
660 Immune Response by Targeting the MAVS signalosome. *Sci Rep* **6**, 22002 (2016).

661 50. L. A. J. O'Neill, A Broken Krebs Cycle in Macrophages. *Immunity* **42**, 393–394 (2015).

662 51. E. L. Mills, *et al.*, Succinate Dehydrogenase Supports Metabolic Repurposing of
663 Mitochondria to Drive Inflammatory Macrophages. *Cell* **167**, 457-470.e13 (2016).

664 52. A. Littlewood-Evans, *et al.*, GPR91 senses extracellular succinate released from
665 inflammatory macrophages and exacerbates rheumatoid arthritis. *J. Exp. Med.* **213**, 1655–
666 1662 (2016).

667 53. L. Cai, *et al.*, Functional impairment in circulating and intrahepatic NK cells and relative
668 mechanism in hepatocellular carcinoma patients. *Clin. Immunol.* **129**, 428–437 (2008).

669 54. Y. T. Bryceson, M. E. March, D. F. Barber, H.-G. Ljunggren, E. O. Long, Cytolytic granule
670 polarization and degranulation controlled by different receptors in resting NK cells. *J Exp*
671 *Med* **202**, 1001–1012 (2005).

672 55. C. Scholtes, *et al.*, Enhancement of genotype 1 hepatitis C virus replication by bile acids
673 through FXR. *J. Hepatol.* **48**, 192–199 (2008).

674 56. F. A. Ran, *et al.*, Genome engineering using the CRISPR-Cas9 system. *Nature Protocols* **8**,
675 2281–2308 (2013).

676 57. Y. Kuang, S. J. Schomisch, V. Chandramouli, Z. Lee, Hexokinase and glucose-6-phosphatase
677 activity in woodchuck model of hepatitis virus-induced hepatocellular carcinoma. *Comp.*
678 *Biochem. Physiol. C Toxicol. Pharmacol.* **143**, 225–231 (2006).

679 58. C. Ramière, *et al.*, Activity of hexokinase is increased by its interaction with hepatitis C
680 virus protein NS5A. *J. Virol.* **88**, 3246–3254 (2014).

681 59. L. Perrin-Cocon, *et al.*, Toll-like Receptor 4-Induced Glycolytic Burst in Human Monocyte-
682 Derived Dendritic Cells Results from p38-Dependent Stabilization of HIF-1α and Increased
683 Hexokinase II Expression. *J. Immunol.* **201**, 1510–1521 (2018).

684 60. J. Payne, J. G. Morris, Pyruvate carboxylase in Rhodopseudomonas spheroides. *J. Gen.*
685 *Microbiol.* **59**, 97–101 (1969).

686 61. M. I. Love, W. Huber, S. Anders, Moderated estimation of fold change and dispersion for
687 RNA-seq data with DESeq2. *Genome Biology* **15**, 550 (2014).

688 62. P. Skehan, *et al.*, New colorimetric cytotoxicity assay for anticancer-drug screening. *J. Natl.*
689 *Cancer Inst.* **82**, 1107–1112 (1990).

690 63. C. Scholtes, *et al.*, High plasma level of nucleocapsid-free envelope glycoprotein-positive
691 lipoproteins in hepatitis C patients. *Hepatology* **56**, 39–48 (2012).

692 64. V. Icard, *et al.*, Secretion of hepatitis C virus envelope glycoproteins depends on assembly
693 of apolipoprotein B positive lipoproteins. *PLoS ONE* **4**, e4233 (2009).

694 65. N. Sonnenschein, M. Geertz, G. Muskhelishvili, M.-T. Hütt, Analog regulation of metabolic
695 demand. *BMC Syst Biol* **5**, 40 (2011).

696 66. N. Sonnenschein, *et al.*, A network perspective on metabolic inconsistency. *BMC Syst Biol*
697 **6**, 41 (2012).

698 67. C. Knecht, C. Fretter, P. Rosenstiel, M. Krawczak, M.-T. Hütt, Distinct metabolic network
699 states manifest in the gene expression profiles of pediatric inflammatory bowel disease
700 patients and controls. *Sci Rep* **6**, 32584 (2016).

701 68. K. Schlicht, *et al.*, The metabolic network coherence of human transcriptomes is associated
702 with genetic variation at the cadherin 18 locus. *Hum. Genet.* **138**, 375–388 (2019).

703 69. P. Nyczka, M.-T. Hütt, Generative network model of transcriptome patterns in disease
704 cohorts with tunable signal strength. *Phys. Rev. Research* **2**, 033130 (2020).

705 70. J. Gao, *et al.*, Integrative Analysis of Complex Cancer Genomics and Clinical Profiles Using
706 the cBioPortal. *Sci Signal* **6**, pl1 (2013).

707 71. E. Cerami, *et al.*, The cBio Cancer Genomics Portal: An Open Platform for Exploring
708 Multidimensional Cancer Genomics Data. *Cancer Discov* **2**, 401–404 (2012).

709

710 **Figures**
711

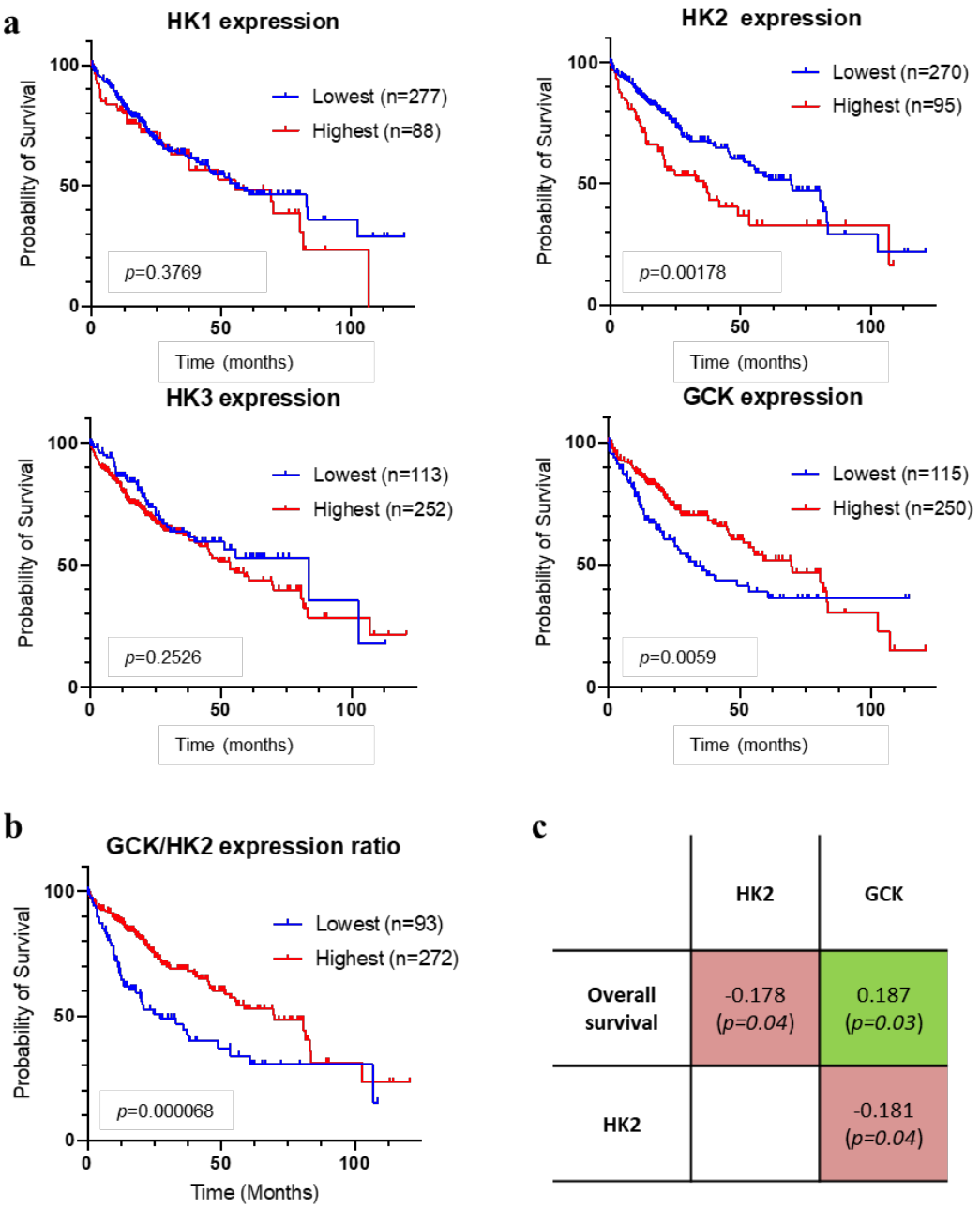

712 **Figure 1. Correlation between hexokinase expression levels in HCC tumors and patient survival.**
713 **a** Kaplan–Meier estimates of the survival of HCC patients depending on the expression of HK1,
714 HK2, HK3 and GCK (HK4) genes in tumor biopsies (n=365; TCGA expression data retrieved from
715 cBioPortal)(70, 71). Duplicate analyses from the same patient were removed as well as patients
716 who died when biopsied (overall survival=0 months). Optimal stratification based on highest and
717 lowest gene expression values was determined using Protein Atlas database (18). **b** Same as above
718 but patients were stratified based on the GCK/HK2 gene expression ratio. The stratification
719 showing the lowest *p* value when comparing subgroups of patients with the highest to the lowest

720 GCK/HK2 expression ratio is displayed. Patient TCGA-DD-AAE9 exhibiting undetectable levels of
721 GCK and HK2 was removed from this analysis as the GCK/HK2 ratio could not be calculated. **c**
722 Correlations between patient survival, GCK expression and HK2 expression. Spearman's rank
723 correlation test on the subset 130 patients for whom the period between diagnosis and death is
724 precisely known (uncensored data).

725

726

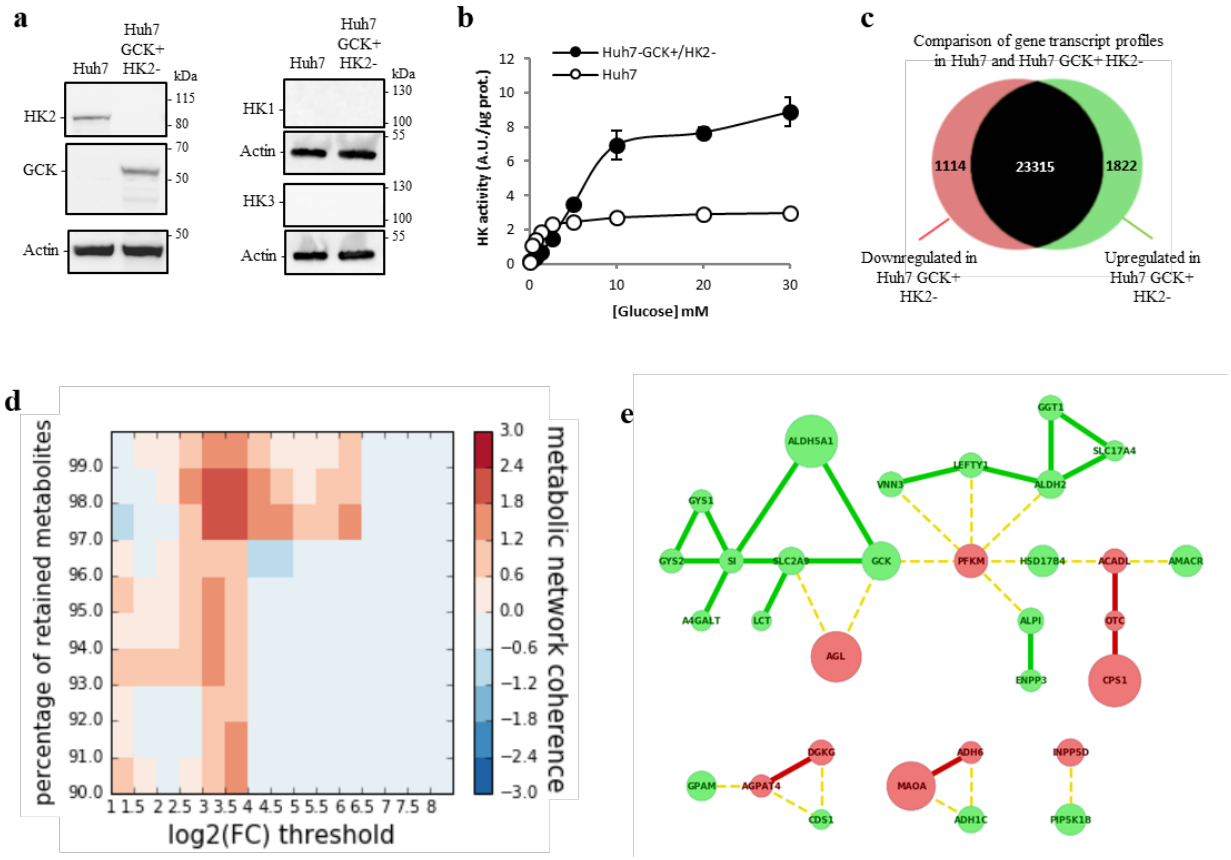

727

728 **Figure 2. Hexokinase isoenzyme switch in Huh7 cells induces extended modifications of**
729 **metabolic connections. a** Western-blot analysis of HK1, HK2, HK3 and GCK expression in Huh7
730 and Huh7-*GCK*$^+$/*HK2*$^-$. **b** Hexokinase activity in homogenates of Huh7 and Huh7-*GCK*$^+$/*HK2*$^-$ cells. **c**
731 Number of genes changing their expression pattern in Huh7 and Huh7-*GCK*$^+$/*HK2*$^-$ cells (see
732 Supplementary Table 2 for details). **d** Heatmap showing clustering enrichment scores of the
733 networks obtained when mapping differentially expressed genes to the human metabolic model
734 Recon2. Clustering enrichment scores from the highest in red to the lowest in blue were
735 calculated for different gene expression thresholds ($Log_2|FC|$) and percentages of retained
736 currency metabolites. **e** Gene network corresponding to the maximal clustering enrichment score
737 ($Log_2|FC|>3$; removed currency metabolites = 2%). The transcription of nodes in green was
738 upregulated and those in red downregulated in Huh7-*GCK*$^+$/*HK2*$^-$ compared to Huh7 cells. Plain

739 edges mark coregulation between nodes and broken edges inverse regulation at the
740 transcriptional level.
741
742

a

Molecular and Cellular Functions		
Name	***p*-value range**	**Number of genes involved**
Cellular Movement	**$7.68 \times 10^{-6} – 4.66 \times 10^{-25}$**	**701**
Lipid Metabolism	**$2.00 \times 10^{-6} – 3.12 \times 10^{-14}$**	**414**
Molecular Transport	$5.63 \times 10^{-6} – 3.12 \times 10^{-14}$	361
Small Molecule Biochemistry	5.63×10^{-6} - 3.12×10^{-14}	462
Protein Synthesis	$1.87 \times 10^{-6} – 3.42 \times 10^{-14}$	199

b

Cellular Movement Functional Annotations		
Name	***p*-value**	**Number of genes involved**
Migration of cells	4.66×10^{-25}	585
Cell movement	3.48×10^{-24}	642
Cell movement of blood cells	1.52×10^{-18}	276
Leucocyte migration	1.59×10^{-18}	274
Invasion of cells	5.33×10^{-17}	306

c

Lipid Metabolism Functional Annotations		
Name	***p*-value**	**Number of genes involved**
Concentration of lipid	3.12×10^{-14}	256
Synthesis of lipid	2.37×10^{-10}	233
Fatty acid metabolism	4.31×10^{-10}	166
Quantity of steroid	4.48×10^{-09}	138
Concentration of cholesterol	6.58×10^{-08}	94

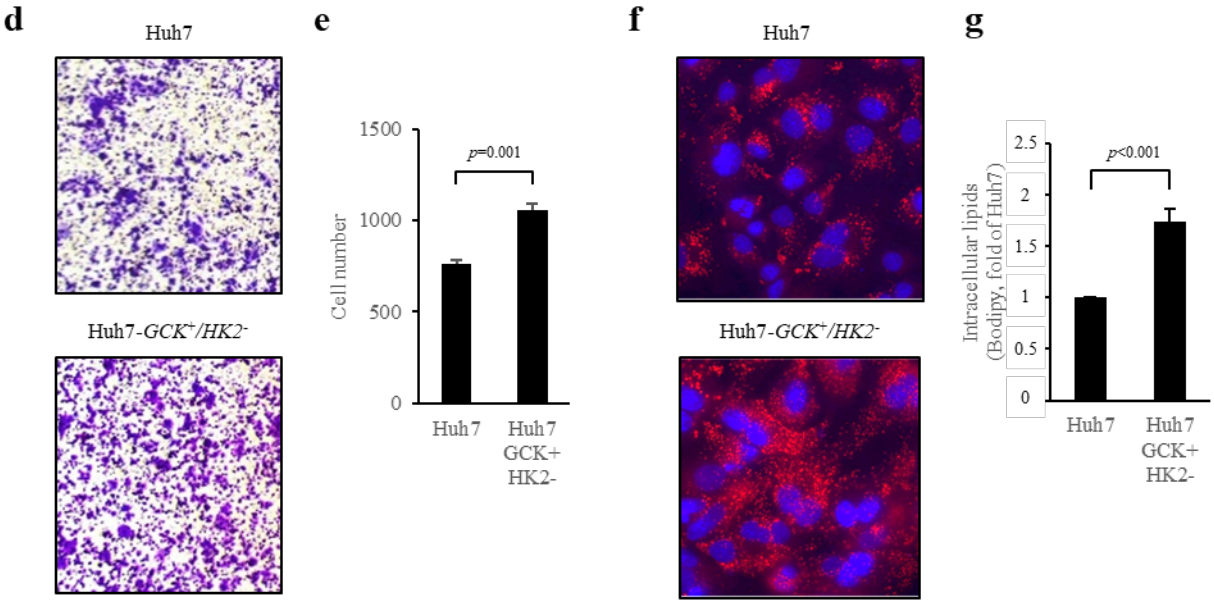

743
744
745 **Figure 3. Huh7-*GCK*$^{+}$/*HK2*$^{-}$ cells have a higher migration capacity and lipid droplets content. a**
746 Analysis of differentially expressed genes in the two cell lines using gene set enrichment analysis
747 (|FC|>2 with a *p* value <0.05). Top five enriched molecular and cellular functions are presented.
748 **b** and **c** Ranked IPA-annotations associated with 'cellular movement' and 'lipid metabolism'. **d, e**

749 Results of transwell-migration tests. **d** Representative images and **e** count of migrating cells. **f** Oil
750 Red-O staining of lipid droplets (red) with nucleus counterstaining (blue). **g** Quantification of
751 intracellular lipids by FACS after BODIPY staining. E and G correspond to means ± SEM with n≥3
752 (*p* value determined by Student's t-test).
753

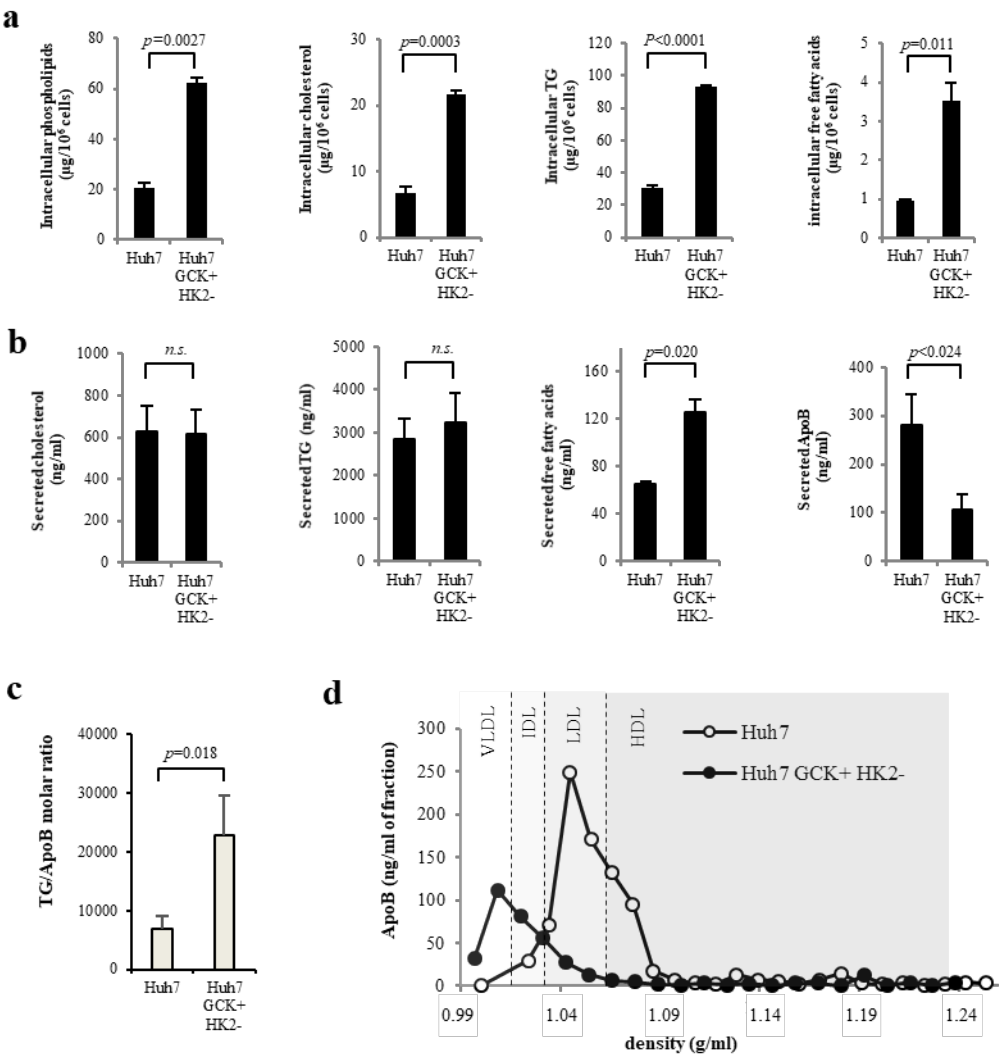

754

755 **Figure 4. Lipogenesis and very-low-density lipoproteins (VLDL) secretion are restored in Huh7-**
756 ***GCK⁺/HK2⁻* cells. a** Quantification of intracellular lipids in total cell extracts of Huh7 and Huh7-
757 *GCK⁺HK2⁻* cells. **b** Lipids and ApoB secretions in supernatants of cells cultured 24h without FCS. **c**
758 TG/ApoB molar ratio calculated from quantifications determined in b. **d** Supernatants of Huh7
759 and Huh7-*GCK⁺/HK2⁻* were analyzed by ultracentrifugation on iodixanol density gradients. ApoB
760 was quantified in each fraction by ELISA. Presented data correspond to means ± SEM (n≥3, *p* value
761 determined by Student's t-test) except for d) that shows one representative experiment.
762

763

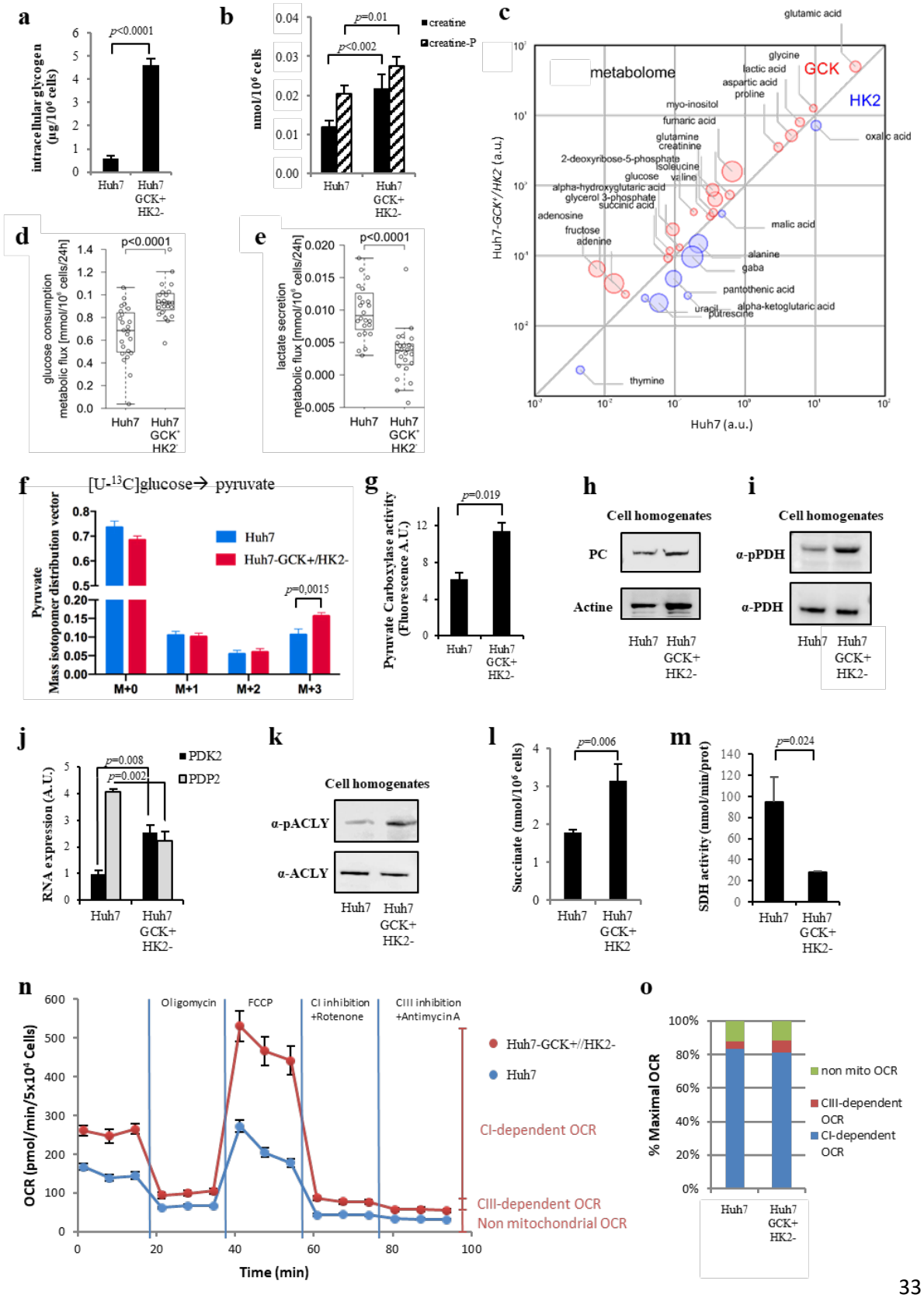
a
intracellular glycogen (µg/10⁶ cells)
p<0.0001
Huh7
Huh7 GCK+ HK2-
b
nmol/10⁶ cells
p=0.01
p<0.002
creatine
creatine-P
Huh7
Huh7 GCK+ HK2-
c
metabolome
GCK
HK2
glutamic acid
glycine
lactic acid
aspartic acid
proline
myo-inositol
fumaric acid
glutamine
creatinine
2-deoxyribose-5-phosphate
isoleucine
glucose
valine
alpha-hydroxyglutaric acid
glycerol 3-phosphate
succinic acid
adenosine
fructose
adenine
oxalic acid
malic acid
alanine
gaba
pantothenic acid
uracil
putrescine
alpha-ketoglutaric acid
thymine
Huh7-GCK+/HK2 (a.u.)
Huh7 (a.u.)
d
glucose consumption metabolic flux [mmol/10⁶ cells/24h]
p<0.0001
Huh7
Huh7 GCK+ HK2-
e
lactate secretion metabolic flux [mmol/10⁶ cells/24h]
p<0.0001
Huh7
Huh7 GCK+ HK2-
f
[U-13C]glucose→ pyruvate
Pyruvate Mass isotopomer distribution vector
Huh7
Huh7-GCK+/HK2-
p=0,0015
M+0
M+1
M+2
M+3
g
Pyruvate Carboxylase activity (Fluorescence A.U.)
p=0.019
Huh7
Huh7 GCK+ HK2-
h
Cell homogenates
PC
Actine
Huh7
Huh7 GCK+ HK2-
i
Cell homogenates
α-pPDH
α-PDH
Huh7
Huh7 GCK+ HK2-
j
RNA expression (A.U.)
p=0.008
p=0.002
PDK2
PDP2
Huh7
Huh7 GCK+ HK2-
k
Cell homogenates
α-pACLY
α-ACLY
Huh7
Huh7 GCK+ HK2-
l
Succinate (nmol/10⁶ cells)
p=0.006
Huh7
Huh7 GCK+ HK2
m
SDH activity (nmol/min/prot)
p=0.024
Huh7
Huh7 GCK+ HK2-
n
OCR (pmol/min/5x10⁴ Cells)
Oligomycin
FCCP
CI inhibition +Rotenone
CIII inhibition +Antimycin A
Huh7-GCK+//HK2-
Huh7
CI-dependent OCR
CIII-dependent OCR
Non mitochondrial OCR
Time (min)
o
% Maximal OCR
non mito OCR
CIII-dependent OCR
CI-dependent OCR
Huh7
Huh7 GCK+ HK2-

764 **Figure 5. TCA rewiring after hexokinase isoenzyme switch in Huh7 cells**. **a** Glycogen
765 quantification. **b** Creatinine and creatinine-P quantification. **c** This bubble chart compares
766 intracellular metabolomes of Huh7 and Huh7-*GCK*$^{+}$/*HK2*$^{-}$ cells. Metabolite pool sizes larger in
767 Huh7 are indicated in blue, whereas the one larger in Huh7-*GCK*$^{+}$/*HK2*$^{-}$ are shown in red. The size
768 of bubbles inversely scales with *p* values between 5.10^{-2} and 1.10^{-17} of differential metabolomics
769 responses. **d, e** Metabolic fluxes for overall glucose consumption (d) and lactate secretion (e) by
770 Huh7 and Huh7-*GCK*$^{+}$/*HK2*$^{-}$ cells. Indicated values correspond to differences in glucose or lactate
771 concentrations in extracellular culture medium before and after 24h of culture. **f** Mass isotopomer
772 distribution vector of pyruvate in cells cultured with [U-^{13}C]-glucose. **g** Pyruvate carboxylase (PC)
773 activity determined in cell homogenates. **h** Western-blot analysis of PC expression in Huh7 and
774 Huh7-*GCK*$^{+}$/*HK2*$^{-}$ cells. **i**) Western-blot analysis of pyruvate dehydrogenase (PDH) E1-alpha subunit
775 phosphorylation at Ser293. **j** RNAseq quantification of pyruvate dehydrogenase kinase 2 (PDK2)
776 and pyruvate dehydrogenase phosphatase 2 (PDP2)(BH adjusted *p* value<0.05 from
777 transcriptomic data). **k** Western-blot analysis of ATP-citrate Lyase (ACLY) phosphorylation at
778 Ser455. **l** Succinate quantification in cell homogenates. **m** Succinate dehydrogenase (SDH) activity
779 determined in cell homogenates. **n** Oxygen consumption rate (OCR) in Huh7 and Huh7-*GCK*$^{+}$/*HK2*$^{-}$
780 cells was determined with a Seahorse analyzer before and after the addition of oligomycin
781 (Complex V inhibitor), FCCP (uncoupling agent), rotenone (Complex I inhibitor) and antimycin A
782 (Complex III inhibitor). **o** Non-mitochondrial, complex I-dependent and complex III-dependent
783 maximal OCR were calculated from n. Data correspond to means ± SEM (n≥3).

a

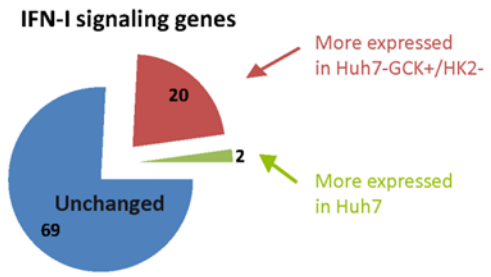

b

Gene ID	Huh7 (mean normalized counts)	Huh7-GCK+/HK2- (mean normalized counts)	FC (calculated by DESeq2 analysis)
EGR1	178,2	537,5	3,0
GBP2	243,0	816,5	3,3
HLA-A	247,2	608,1	2,5
HLA-B	13,4	29,8	2,2
HLA-H	177,8	579,0	3,3
HSP90AB1	0,0	622,9	10000,0
IFI35	50,2	252,5	5,0
IFI6	21,7	142,8	6,6
IFIH1	34,5	106,1	3,1
IFITM3	180,9	1081,4	6,0
IKBKE	0,3	419,4	1284,3
IRF1	212,9	505,2	2,4
IRF3	38,5	84,4	2,2
IRF9	109,3	388,8	3,6
ISG15	89,9	197,6	2,2
MX1	0,0	28,6	10000,0
OAS1	0,8	157,5	173,5
OAS3	195,1	1095,0	5,6
PSMB8	0,0	13,4	80,0
RNASEL	0,0	4,9	10000,0
ABCE1	6559,7	3037,7	-2,2
TRIM6	663,1	263,9	-2,5

c

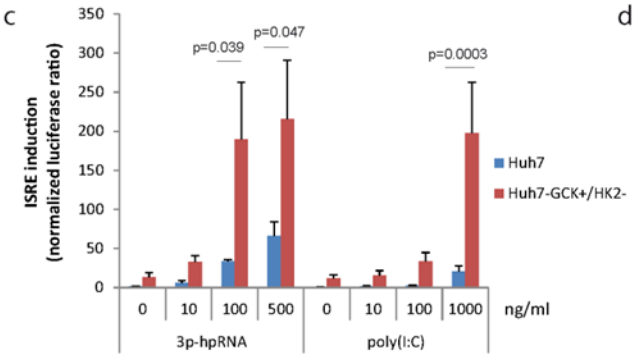

d

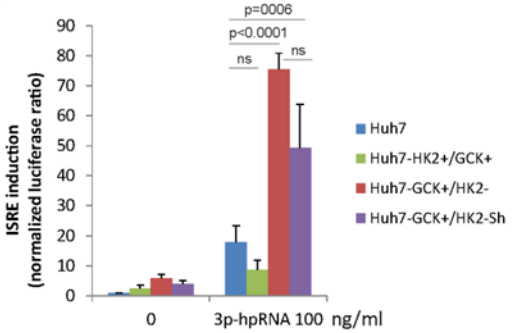

e

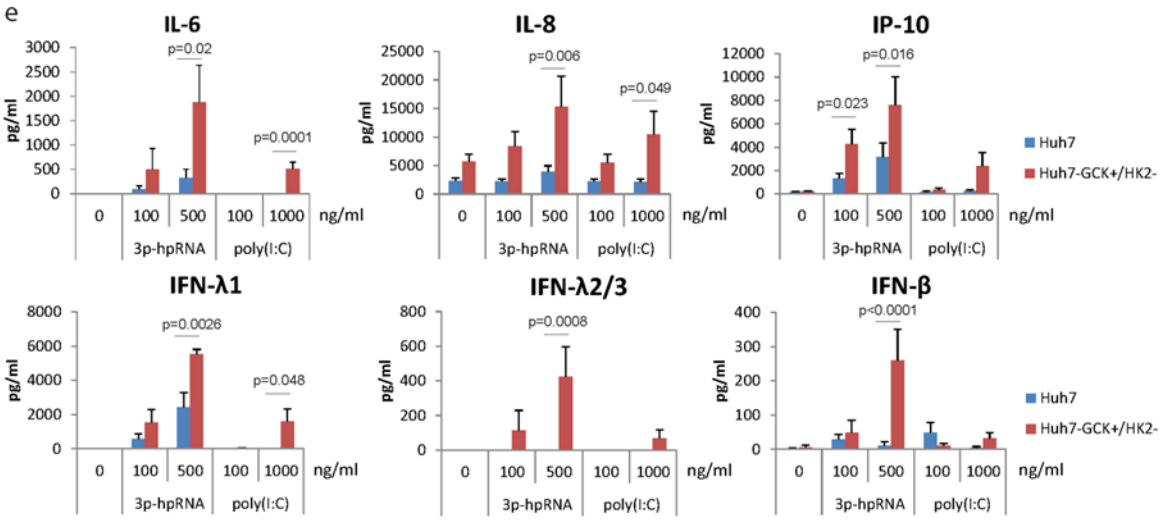

f

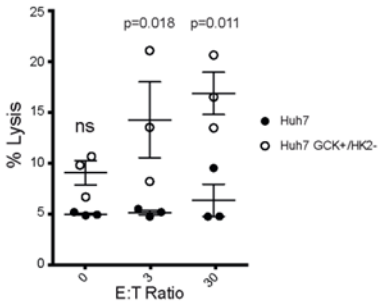

785 **Figure 6. Innate immune response is enhanced in Huh7-GCK$^+$/HK2$^-$ cells. a** Sector chart from the
786 transcriptomic study showing genes included in the GO-term "Type I-IFN signaling pathway". **b**
787 List of genes significantly up-regulated in purple or down-regulated in green (|FC|>2, BH adjusted
788 *p* value<0.05) in Huh7-*GCK$^+$/HK2$^-$*compared to Huh7 cells. **c-e** Cells were stimulated or not for 48h
789 with 3p-hpRNA (RIG-I ligand) or poly(I:C) (IFIH1/MDA5 ligand). ISRE-luciferase expression was
790 monitored and normalized to Renilla luciferase (c, d). Cell supernatants were assayed for cytokine
791 concentration by multiplex assays (e). **f** NK cell mediated lysis of Huh7 or Huh7-*GCK$^+$/HK2$^-$*.
792 Hepatoma cells were seeded 24h before NK cells addition for 4h at effector to target (E:T) ratio of
793 0, 3 or 30. After harvesting, cell lysis was determined by the percentage of PI+ cells on gated
794 hepatocytes. *p* values were obtained from 2-way ANOVA analyses comparing matched cell means
795 with Sidak's correction for multiple comparison, with α=0.05.

796

797

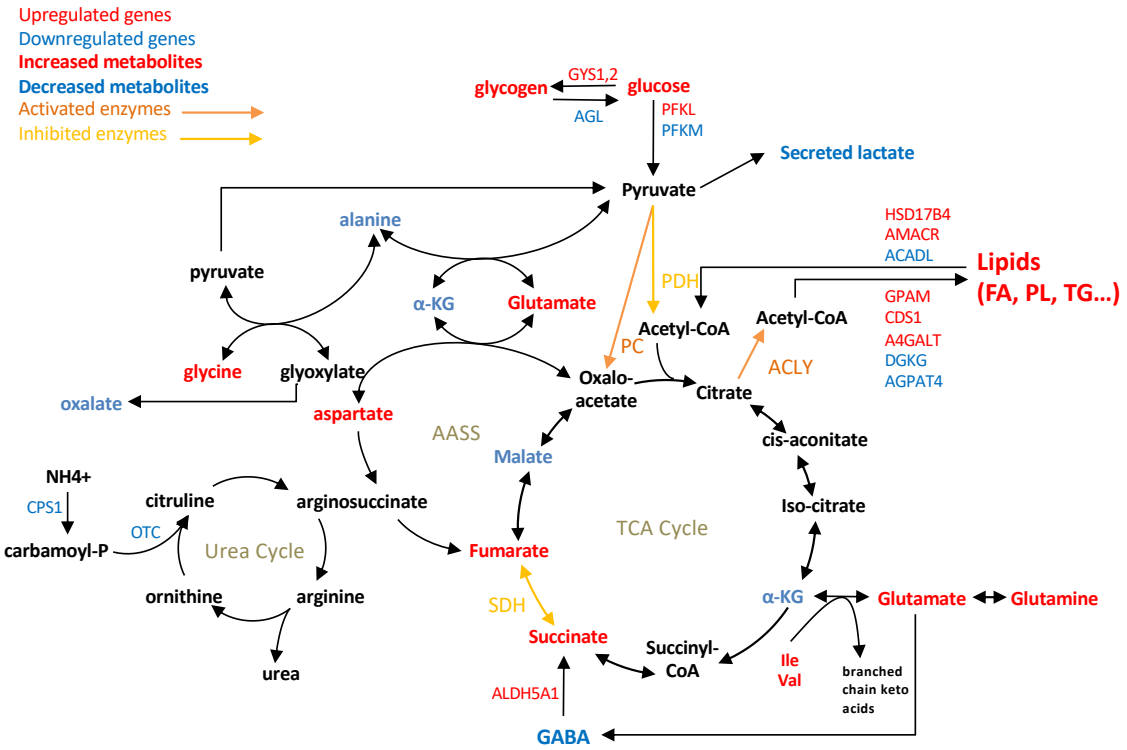

Figure 7. Simplified scheme of central carbon metabolism and connected pathways showing differences between Huh7-*GCK*$^{+}$/*HK2*$^{-}$ vs Huh7. Highlighted metabolites, enzymatic activities, and metabolism-associated genes were selected from transcriptomic (Fig. 2e), metabolomic (Fig. 5c) and enzymatic analyses (Fig. 5g-m).